Axionlike dark matter search using the storage ring EDM method

Seung Pyo Chang,[1,2] Selçuk Hacıömeroğlu,[2] On Kim,[1,2] Soohyung Lee,[2] Seongtae Park,[2,*] and Yannis K. Semertzidis[1,2]

[1]*Department of Physics, KAIST, Daejeon 34141, Republic of Korea*
[2]*Center for Axion and Precision Physics Research, IBS, Daejeon 34051, Republic of Korea*

We propose using the storage ring electric dipole moment (EDM) method to search for the axion dark matter induced EDM oscillation in nucleons. The method uses a combination of B and E fields to produce a resonance between the $g-2$ spin precession frequency and the background axion field oscillation to greatly enhance sensitivity to it. An axion frequency range from 10^{-9} Hz to 100 MHz can, in principle, be scanned with high sensitivity, corresponding to an f_a range of 10^{13} GeV $\leq f_a \leq 10^{30}$ GeV, the breakdown scale of the global symmetry generating the axion or axionlike particles.

I. INTRODUCTION

Peccei and Quinn proposed a dynamic oscillating field to solve the strong CP problem [1], and that oscillating field is called an axion [2–8]. An axion in the parameter range of 10^{11} GeV $\leq f_a \leq 10^{13}$ GeV is potentially observable using microwave cavity resonators, where f_a is the global symmetry breakdown scale [9–12]. This method detects photons from the axion dark matter conversion in the presence of strong magnetic fields [10,13–16]. In the next decade, it is expected that the axion frequency range of 0.1–50 GHz may be covered using microwave cavity and/or open cavity resonators [17]. However, this method cannot be used for higher values of f_a (lower mass region), because the axion-photon coupling is suppressed by f_a ($\sim 1/f_a^2$) and the required resonance structures would be impractically large. For the higher values of the scale, including M_{GUT} ($\sim 10^{16}$ GeV)-M_{PL} ($\sim 10^{19}$ GeV), axion-gluon coupling can be considered, which gives a time-varying electric dipole moment (EDM) to nucleons [11,12]. For example, in the nucleon case, the EDM can be expressed as

$$d_n = 2.4 \times 10^{-16} \frac{a}{f_a} \sim (9 \times 10^{-35}) \cos(m_a t) \ [e \cdot \mathrm{cm}], \quad (1)$$

$$a(t) = a_0 \cos(m_a t), \quad (2)$$

where $a(t)$ is the axion dark matter field and m_a is the axion mass. Graham and Rajendran proposed a method that

*Corresponding author.
stpark@ibs.re.kr

measures the small energy shift with the form $\vec{E} \cdot \vec{d}_n$ in an atom as a probe of the oscillating axion field [11]. In this case, the electric field is an internal atomic field. By combining Eqs. (1) and (2) with a possible static EDM, one can write the total EDM as

$$d(t) = d_{dc} + d_{ac} \cos(m_a t + \varphi_{ax}), \quad (3)$$

where d_{dc} and d_{ac} are the magnitudes of the static and oscillating parts of EDM, respectively, and φ_{ax} is the phase of the axion field. In this paper, we propose using the storage ring technique to probe the oscillating EDM signal [18–20], with some modification of storage ring conditions depending on the axion frequency. Instead of completely zeroing the $g-2$ frequency, we just control and tune it to be in resonance with the axion background field oscillation frequency. We propose searching for the oscillating EDM term by using a resonance with the $g-2$ precession frequency. This method is expected to be more sensitive, and the systematic errors are easier to handle than in the frozen spin storage ring EDM method. Using the storage ring method, one can scan the frequency range from 10^{-9} Hz up to 100 MHz, which corresponds to an axion parameter space of about 10^{13} GeV $\leq f_a \leq 10^{30}$ GeV.

The particle (or field) discussed in this paper is not the exact QCD axion. However, we use the term axion for both axions and axionlike particles without distinguishing them throughout the paper.

II. RESONANCE OF AXION-INDUCED OSCILLATING EDM WITH $g-2$ SPIN PRECESSION IN STORAGE RINGS

The previously proposed storage ring EDM experiment is optimized for a dc (fixed in time) nucleon EDM, applied to protons and deuterons [18–20]. It is designed to keep

(freeze) the particle spin direction along the momentum direction for the duration of the storage time, typically for 10^3 s, the stored beam polarization coherence time [20,21]. In this case, the radial electric field in the particle rest frame is precessing the particle spin in the vertical plane. The precession frequency in the presence of both E and B fields is expressed by the Thomas-BMT (Bargmann-Michel-Telegdi) Eqs. (4)–(6) [22,23]:

$$\vec{\omega} = \vec{\omega}_G + \vec{\omega}_d, \tag{4}$$

$$\vec{\omega}_G = -\frac{e}{m}\left[G\vec{B} - \left(G - \frac{1}{\gamma^2 - 1}\right)\frac{\vec{\beta} \times \vec{E}}{c}\right], \tag{5}$$

$$\vec{\omega}_d = -\frac{e}{m}\left[\frac{\eta}{2}\left(\frac{\vec{E}}{c} + \vec{\beta} \times \vec{B}\right)\right], \tag{6}$$

where $G = (g - 2)/2$ is the magnetic anomaly with $G = -0.14$ for deuterons. Here, other terms are omitted by assuming the conditions $\vec{\beta} \cdot \vec{E} = \vec{\beta} \cdot \vec{B} = 0$. The parameter η shown in the equation is related to the electric dipole moment d as $d = \eta e\hbar/2mc$. Since we are dealing with a time-varying EDM due to the oscillating axion background field, η is also a function of time. The $\vec{\omega}_G$ is the angular frequency, i.e., 2π times the $g - 2$ frequency, describing the spin precession in the horizontal plane relative to the momentum precession.

The term $\vec{\omega}_d$ is due to the EDM and the corresponding precession takes place in the vertical plane. For a time-independent nucleon EDM, the spin vector will precess vertically for the duration of the storage time if the horizontal spin component is fixed to the momentum direction [20]. This condition can be achieved by setting the E and B fields properly and is called the frozen spin condition.

With a nonzero $g - 2$ frequency, the average EDM precession angle becomes zero for the static EDM case, because the relative E-field direction to the spin vector changes within every cycle of $g - 2$ precession. For example, the spin tilts in one direction (up or down) due to the EDM within one half cycle and then tilts in the opposite direction for the other half cycle, resulting in an average accumulation of zero. The presence of a static EDM will only slightly tilt the $g - 2$ precession plane away from the horizontal plane, without a vertical spin accumulation. In contrast, for an oscillating EDM, when the axion frequency (ω_{ax}) is the same as the $g - 2$ frequency with the appropriate phase, the precession angle can be accumulated in one direction. This is possible because the EDM direction flips every half cycle due to the axion field oscillation and the relative direction between the E field and the EDM d always remains the same.

In this idea of resonant axion-induced EDM with $g - 2$ spin precession, one can utilize the strong effective electric field $\vec{E}^* = \vec{E} + c\vec{\beta} \times \vec{B}$, which comes from the B field due to particle motion, as expressed in Eq. (6). In this case, the effective electric field is about 1 or 2 orders of magnitude larger than the applied external E field, which can be up to 10 MV/m and has an apparent technical limitation in strength.

III. SENSITIVITY CALCULATION

The statistical error in the EDM for proton or deuteron can be expressed with the following equation [19,20]:

$$\sigma_d = \frac{2\hbar s}{PAE^*\sqrt{N_c \kappa T_{\text{tot}}\tau_p}}, \tag{7}$$

where P is the degree of polarization, A the analyzing power, E^* the effective electric field that causes the EDM precession, N_c the number of particles stored per cycle, κ the detection efficiency of the polarimeter, τ_p the polarization lifetime, and T_{tot} the total experiment running time. The s in the numerator is $1/2$ for protons and 1 for deuterons. One can easily calculate the sensitivity of nucleon EDM measurement using this formula with the corresponding experimental parameters.

In this study, we used the following method to calculate the sensitivities of the axion EDM measurement including the oscillation effect. First, we chose the target axion frequency and then calculated the corresponding E and B fields for the particle storage, which give the same $g - 2$ frequency as the chosen axion frequency. Then, the axion oscillation and $g - 2$ spin precession will be on resonance, and the EDM precession angle in the vertical plane can keep accumulating during the measurement time. With the chosen axion frequency and the axion quality factor Q_{ax}, we estimated the statistical error, and the resulting error was used to calculate the experiment sensitivity along with the effective electric field. This method can be used not only for nucleons like deuterons or protons but also for other leptonic particles like muons, provided there is a coupling between the oscillating θ_{QCD} induced by the background axion dark matter field and the particle EDM.

As shown in Eq. (6), the EDM part of the precession rate can be rewritten as

$$\omega_d = \frac{d\theta}{dt} = -\frac{d}{s\hbar}E^*,$$
$$E^* = E + c\beta B, \tag{8}$$

where s is $1/2$ for protons and 1 for deuterons. Accordingly, $d = \frac{s\hbar}{E^*}\omega_d$, and the error for the EDM d can be written as

$$\sigma_d = \frac{s\hbar}{E^*}\sigma_{\omega_d}, \tag{9}$$

where σ_{ω_d} is the error for ω_d. It can be obtained from the fit of the vertical precession angle θ as a function of time.

The time variation of $\theta(t)$ will be obtained from the asymmetry $\epsilon(t)$ measurement (explained below) using a polarimeter [24–28]. For the hadronic particle case, one can utilize the nuclear interactions between the spin-polarized particles and target nuclei. In this case, the spin-orbit interaction between the spin-polarized incident particle and target nucleus is one of the major reactions that gives asymmetrical scattering of the incident particle in the azimuthal angle [29]. Carbon is one of the most efficient target materials with a large analyzing power for both deuterons and protons.

For example, the scattering cross section for a spin-1/2-polarized particle (e.g., a proton) can be written as [25]

$$I(\psi, \phi) = I_0(\psi)[1 + p_y A_y(\psi)], \qquad (10)$$

where $I_0(\psi)$ is the cross section for an unpolarized particle scattered into the angle ψ, $A_y(\psi)$ is the analyzing power of the reaction, and $p_y = p_\perp \cos(\phi)$ is the y component of the beam polarization. $p_\perp$ is the component of beam polarization perpendicular to the particle momentum. From Eq. (10), the number of hits recorded in a detector located at (ψ, ϕ) can be written as follows:

$$N(\psi, \phi) = n N_A \Delta\Omega \zeta I(\psi, \phi), \qquad (11)$$

where n is the number of particles incident on the target, N_A is the number of target nuclei per square centimeter, $\Delta\Omega$ is the solid angle subtended by the detector, and ζ is the efficiency of the detector. If we assume identical detectors which are placed at symmetrical locations on the left and right of the beam direction, the counts recorded on the left and right are

$$L \equiv N(\psi, 0) = n N_A \Delta\Omega \zeta I_0(\psi)[1 + p_\perp A_y(\psi)] \qquad (12)$$

and

$$R \equiv N(\psi, \pi) = n N_A \Delta\Omega \zeta I_0(\psi)[1 - p_\perp A_y(\psi)], \qquad (13)$$

respectively. After simple algebra, one can obtain the left-right asymmetry ϵ for the vertically polarized beam as follows:

$$\epsilon(t) = \frac{L - R}{L + R}(t) = pA\theta(t), \qquad (14)$$

where A is the analyzing power, $\theta(t)$ is the accumulated EDM precession angle in the vertical plane, and L and R are the number of hits on the left and right detectors, respectively. Here we replaced the notation $p_\perp$ with p. As mentioned earlier, one can get the EDM precession rate ω_d from the asymmetry $\epsilon(t)$.

The axion quality factor depends on the model used for the calculation. In this paper, we used the axion quality factor of $Q_{ax} = 3 \times 10^6$ in reference to numbers from two theory papers [30,31]. From the Q_{ax} value, one can calculate the possible measurement time $t_m = Q_{ax}/f_{ax}$

(coherence time between the axion oscillation and $g - 2$ spin precession), where f_{ax} is the axion frequency [11]. If this time t_m is larger than the polarization lifetime t_{pol} [or spin coherence time (SCT)], then we set the measurement time to t_{pol}. Otherwise, the measurement time is set to Q_{ax}/f_{ax}. Furthermore, in some models, the oscillating axion field is monochromatic with a quality factor in excess of 10^{10}; see Refs. [32,33], and references therein. As shown in Table I in the Appendix, with this high Q_{ax} value, one can reach very high sensitivities up to $10^{-31,-32} e \cdot$ cm under the said assumptions.

In resonance microwave cavity experiments, the conversion power of axion to photon is limited by the cavity quality factor Q_L. Therefore, there is no large benefit from the high axion Q_{ax} value if the cavity Q_L is smaller than the axion Q_{ax} value. The current cavity experiment assumes the axion Q_{ax} to be about a few times 10^6, and the cavity Q_L is usually smaller than this. However, the proposed storage ring method can obtain a large benefit from the large Q_{ax} value, since the spin tune stability in the storage ring becomes very large and the sensitivity is even more enhanced with higher Q_{ax} values, as shown in Tables I and II. For example, it was experimentally measured at COSY that the spin tune was controllable at the precision level of 10^{-10} for a continuous 10^2 s accelerator cycle time [34].

A. Pure magnetic ring

The effective electric field is an important parameter in the sensitivity estimation. As shown in Eq. (6), $\vec{E}^*$ is the vector sum of the radial $\vec{E}$ field and $\vec{v} \times \vec{B}$. For this study, we started with a pure magnetic ring first. We assumed the ring bending radius to be $r = 10$ m. In order to tune the $g - 2$ frequency f_{g-2} (or axion frequency on the resonance condition), the B field was varied, and the momentum was also changed accordingly to keep the ring bending radius unchanged. The bottom right plot in Fig. 1 shows the sensitivity as a function of the $g - 2$ frequency, and Eq. (7) is used for the calculation. As can be seen in the plot, the experiment is more sensitive at high frequencies. This is because the larger B field provides a larger effective E field by $\vec{v} \times \vec{B}$. Below $\sim 10^5$ Hz, the sensitivity decreases beyond $\geq 10^{-29} e \cdot$ cm. We decided to use the E and B field combined ring for the low-frequency region to improve the sensitivity in that range.

B. E/B combined ring

The B field was set to 0.38 T, and the E field was applied to the radial direction (radially outwards indicates positive direction) as shown in Fig. 2(a). Figure 2(b) shows the $g - 2$ frequency as a function of the applied E field. To increase the frequency, the E field has to be reduced. However, with this E-field change, the ring radius changes as well. In order to keep the ring radius unchanged
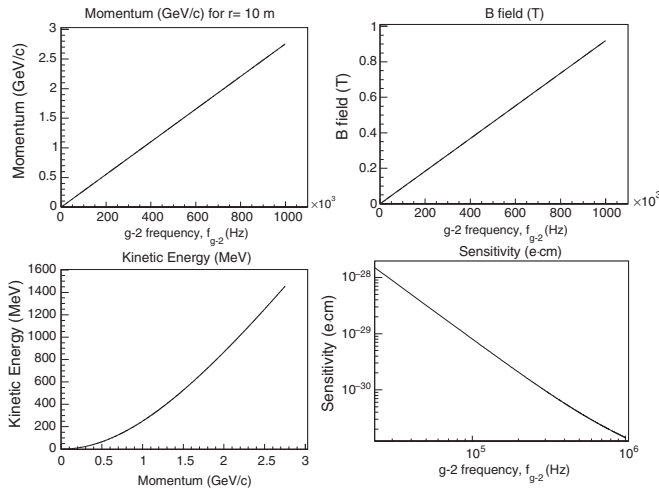
FIG. 1. Deuteron sensitivity vs $g-2$ frequency (or axion frequency). Purely magnetic ring only with ring bending radius $r = 10$ m.

($r = 10$ m for the deuteron in this example), the momentum is adjusted accordingly. Some examples of the experimental conditions are listed in Table I.

Using the parameters shown in Table I, we generated the asymmetry data, and the data were fit to a function which is a combination of a linear function and an exponential function reflecting polarization decay. From the fit, we obtained the error for the precession frequency, σ_{ω_d}. The fit error was inserted into Eq. (9) to calculate the error of the EDM d.
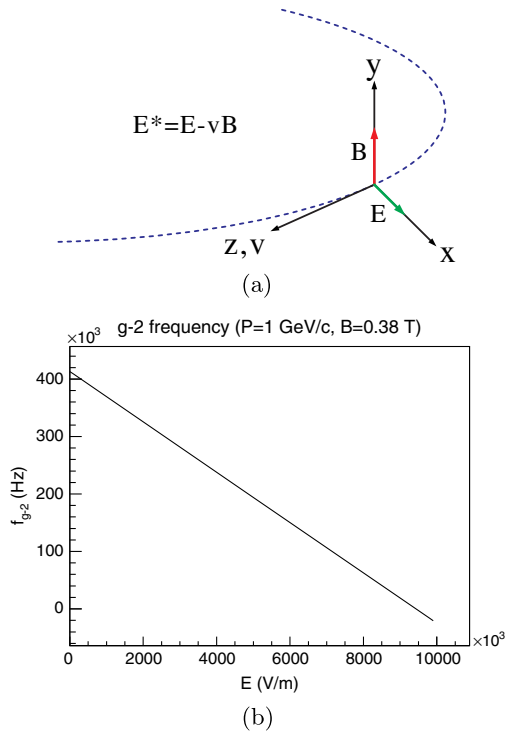

FIG. 2. E/B combined ring for $g-2$ frequency tuning. (a) The coordinate of B, E and ν. (b) $g-2$ frequency vs E field.

In order to observe changes in the vertical spin direction due to EDM precession, only two measurements, at an early time and a later time, are required by spending half of the total particles for each measurement. By using as many particles as possible for two points, an optimum error can be obtained. However, we used 20% of the particles in this simulation to monitor the spin status during the measurement.

An example of the simulation result with the fit is shown in Fig. 3. In the simulation, 40% of the particles were extracted in the early 10% of measurement time (or storage time), and another 40% were extracted in the late 10% of measurement time. The remaining 20% of the particles were extracted in the middle 80% measurement time. The middle 80% of time can be used to measure the $g-2$ frequency. The calculated sensitivities are also shown in Table I for the deuteron case and are all about $10^{-30} e \cdot$ cm or less.

The polarimeter efficiency and the average analyzing power used for the sensitivity calculation were 2% and 0.36, respectively, for the deuteron case (Table I). The numbers are for the elastic d-C reaction (exclusive reaction) measured at the deuteron energy of 270 MeV ($p = 1042$ MeV/c) [35]. The analyzing power is a function of the particle energy, and one should avoid the energies that have small analyzing powers. For a frequency of 1 MHz, the required momentum is about 2.8 GeV/c ($T \sim 1.5$ GeV) for a magnetic field of 0.92 T, as shown in Table I. In the literature [36], one can find corresponding analyzing powers for the inclusive d-C reaction to be maximum about 0.15 within the angle range we are interested in, 5°–20°. This value is still practically useful, but beyond this momentum the analyzing power might be too small to be used for the deuteron polarization analysis.

We repeated the estimations for the proton case as well, and the results are shown in Table II. For the proton, we assumed the ring bending radius to be 52 m. This is the ring
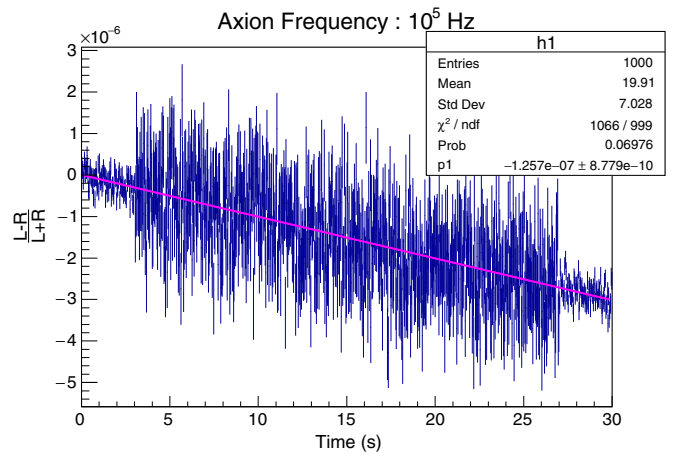

FIG. 3. Simulation result of asymmetry vs time with fit.

radius value suggested for the static EDM measurement by the storage ring proton EDM Collaboration [20]. The proton has a larger magnetic anomaly ($G = 1.79$) than the deuteron, and its mass is half that of the deuteron. Therefore, its spin precession rate in the magnetic field is about 26 times more sensitive than the deuteron case. For this reason, small magnetic fields have to be used for a low axion frequency scan. Because of the small magnetic field (contributing to effective electric field E^*), the calculated sensitivities are not as good as in the deuteron case. However, the resulting sensitivities are still comparable to the static EDM case ($\sim 10^{-29} e \cdot$ cm). Instead of varying the electric field strength (as was done for the deuteron case), the magnetic field was changed to modify the $g - 2$ frequency. We changed the momentum as needed to keep the same ring radius. However, we kept the proton kinetic energy at around 200 MeV ($P \geq 650$ MeV/c) to keep a large analyzing power from the polarimeter detector. The average analyzing power for a proton energy of about 200 MeV is about 0.6 [37], and this value was used in the sensitivity estimation as shown in Table II.

The last two rows in Table II are for the presence of a B field only, and the ring bending radius used was $r = 10$ m. A high frequency ($\geq 10^7$ Hz) can be easily reached at small B fields. However, for a constant ring bending radius, the momentum has to be changed. When the proton case is combined with the deuteron results shown in Table I, one can perform measurements from 10^{-9} Hz to 100 MHz using the same storage ring with a bending radius of $r = 10$ m.

IV. AXION PHASE EFFECT

Since the initial phase of the axion field is unknown, the phase φ_{ax} that appears in Eq. (3) cannot be controlled in the experiment. However, the rate of the EDM precession angle strongly depends on the relative phase between the initial spin and axion phase φ_{ax}. Figure 4 shows the effect of
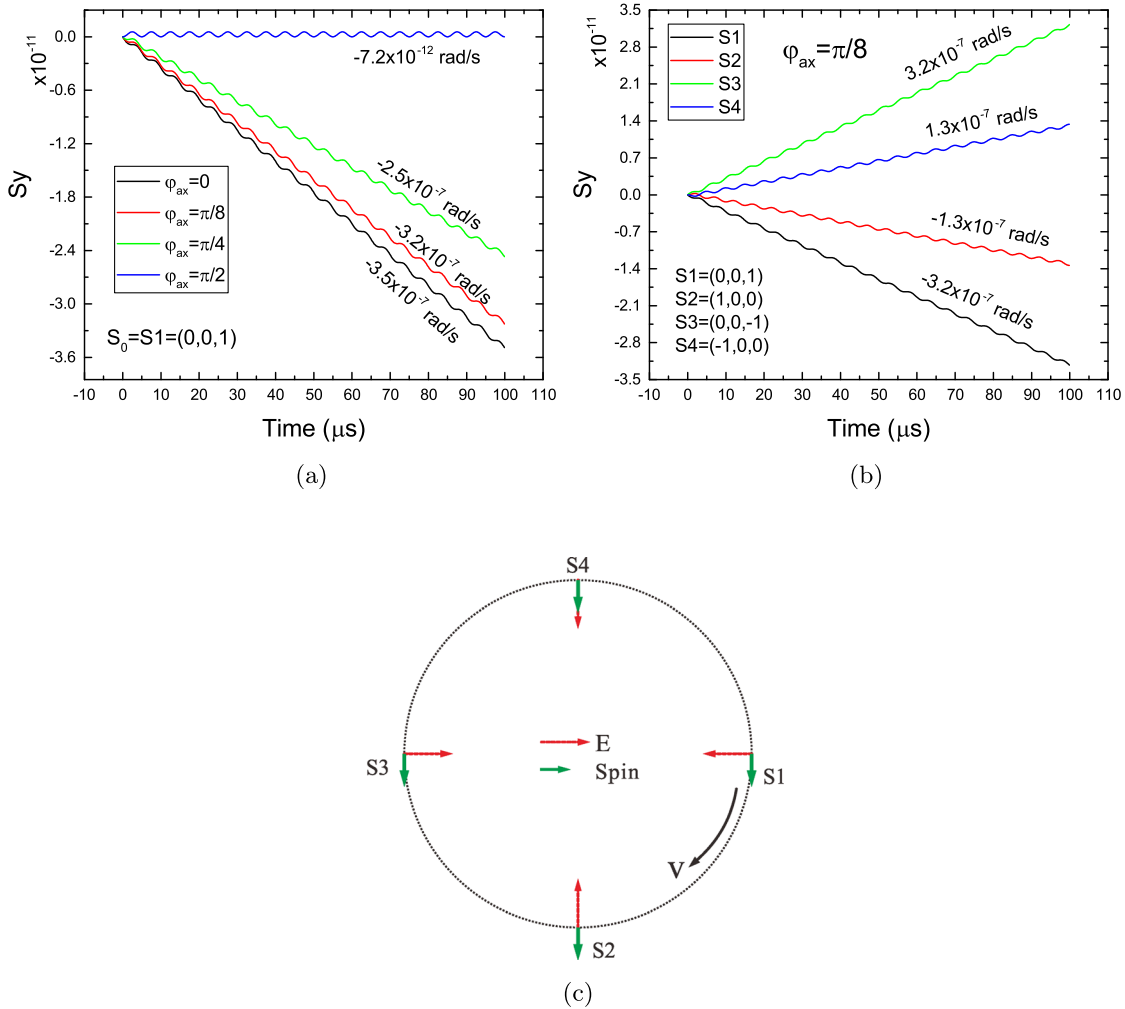

FIG. 4. Axion phases and EDM precession rates. (a) Axion phase dependence of EDM precession rates. (b) Spin polarization dependence of EDM precession rates. Initial axion phase $\varphi_{ax} = \pi/8$. (c) Example of four orthogonal spin polarization settings.

initial phase on the vertical spin precession (EDM effect). The parameters used in the simulation are for an axion frequency of 10^5 Hz, which is shown in Table I. The spin tracking was done by integrating the following two equations [22,23] for spin and velocity, respectively:

$$\frac{d\vec{s}}{dt} = \frac{e}{m}\vec{s} \times \left[\left(\frac{g}{2} - \frac{\gamma-1}{\gamma} \right) \vec{B} \right.$$

$$- \left(\frac{g}{2} - 1 \right) \frac{\gamma}{\gamma+1}(\vec{\beta} \cdot \vec{B})\vec{\beta} - \left(\frac{g}{2} - \frac{\gamma}{\gamma+1} \right) \frac{\vec{\beta} \times \vec{E}}{c}$$

$$\left. + \frac{\eta}{2} \left(\vec{\beta} \times \vec{B} + \frac{\vec{E}}{c} - \frac{\gamma}{\gamma+1}\frac{\vec{\beta} \cdot \vec{E}}{c}\vec{\beta} \right) \right], \tag{15}$$

$$\frac{d\vec{\beta}}{dt} = \frac{e}{\gamma m}\left[\vec{\beta} \times \vec{B} + \frac{\vec{E}}{c} - \frac{\vec{\beta} \cdot \vec{E}}{c}\vec{\beta} \right]. \tag{16}$$

As can be seen in Fig. 4(a), the vertical EDM precession rates are different depending on the initial axion phases. However, this arbitrary axion phase problem can be solved using two (or four) spin-polarized beam bunches with a fixed phase relationship between bunches. An example of four beam bunches with initial spin polarization indicated by short arrows is shown in Fig. 4(c). The figure shows the phase relationship between each spin relative to the electric field. The phase of $S1$ is $\pi/2$ ahead of the E field, π for $S2$, $3\pi/2$ for $S3$, and so on. While the direction of the electric field is fixed to the ring center, the spins precess with $g-2$ frequency during circulation in the ring. However, the relative phase difference between four bunches of beam polarization is always the same during the precession.

Figure 4(b) shows four different initial spin polarization effects for ω_{EDM} in the case of $\varphi_{ax} = \pi/8$. From the measurement of individual spin polarization, the total EDM precession rate can be calculated using the relationship $\omega_{\mathrm{EDM}} = \sqrt{\omega_{\mathrm{EDM},S1}^2 + \omega_{\mathrm{EDM},S2}^2}$, where $\omega_{\mathrm{EDM},S1}$ and $\omega_{\mathrm{EDM},S2}$ are precession rates for the two sets of polarizations $S1$ and $S2$, respectively, with a $\pi/2$ phase difference relative to the electric field as shown in Fig. 4(c). The corresponding axion phase can be obtained by $\varphi_{ax} = \arctan(\frac{\omega_{\mathrm{EDM},S2}}{\omega_{\mathrm{EDM},S1}})$. As can be seen in the example shown in Fig. 4(b), the $S1$ and $S3$ states have large precession rates $(3.2 \times 10^{-7}$ rad/s$)$ for the axion phase of $\varphi_{ax} = \pi/8$, and the precession directions are opposite to each other. On the other hand, note that the other two polarizations $S2$ and $S4$ have smaller ω_{EDM} than the two counterparts of the polarizations ($S1$ and $S3$). In any case, the actual precession rate ω_{EDM} can be calculated using the formula shown above.

Figure 5 shows a simulation result for deuteron spin precession in an E/B combined ring with 100 kHz of $g-2$ frequency. The electric and magnetic fields used in the simulation were 7.05×10^6 V/m and 0.38 T, respectively.
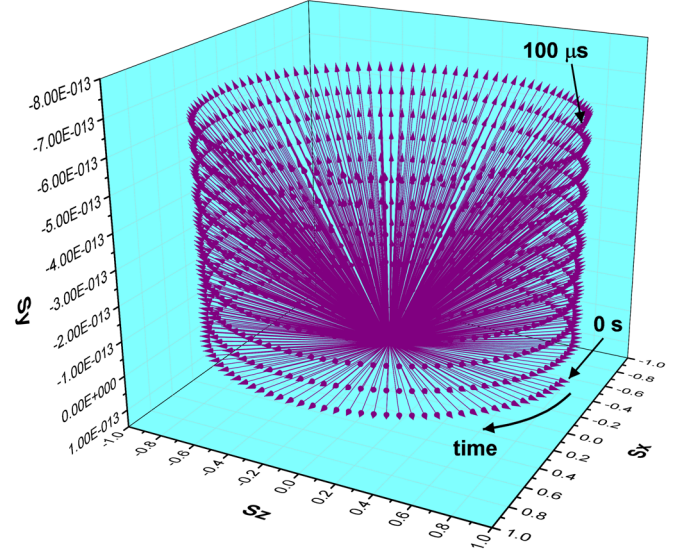

FIG. 5.   Deuteron spin precession in an E/B combined ring.

The initial spin direction was set to the $+z$ direction $(0,0,1)$, and the total precession time shown in the figure is 100 μs. As can be seen, the vertical spin component (S_y) is accumulated, while the horizontal spin precession takes place at the $g-2$ frequency. As mentioned before, the vertical precession rate depends on the initial axion phase.

The induced EDM due to the θ_{QCD} has been calculated to be 3 times larger for the proton than that for the deuteron [18,19]. This means that the proton EDM described by Eq. (1) is 3 times larger than the deuteron case [38]. However, in this sensitivity estimation, we used the same EDM d for both the deuteron and the proton.

V. SCANNING METHOD

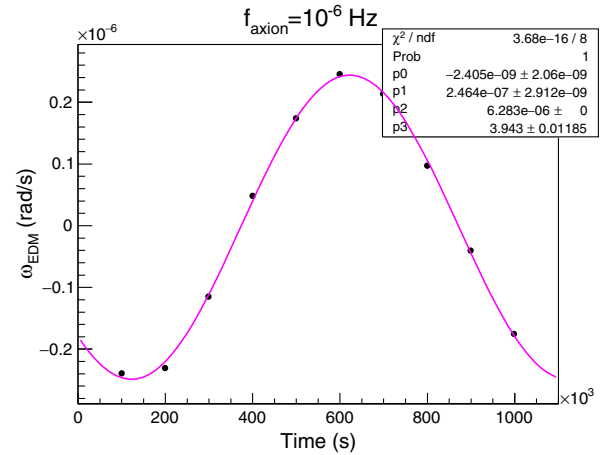The sensitivities presented in Tables I and II are based on the assumption that we know the axion mass (frequency)

FIG. 6. $\omega_{\mathrm{EDM}}(t)$ measurement with the frozen spin condition. The data are fit to the sine function for the sensitivity calculation.

and perform the measurement at the same frequency for 8×10^7 s. However, since we do not know the axion mass yet, all the possible frequency ranges have to be searched for. We used different scan methods for different frequency regions.

For very low frequencies, $f_{ax} < 100~\mu$Hz, one can use the frozen spin method, which was used for the static EDM search, parasitically. With this method, one can take data repeatedly from the frozen spin condition for a limited storage time. The storage time has to be smaller than the axion coherence time and spin coherence time. For example, assuming a spin coherence time of 10^4 s, one can use 10^4 s as the maximum storage time, and with this storage time one can test up to $100~\mu$Hz.

Figure 6 shows an example of simulation results for an axion frequency of $1~\mu$Hz. Each point corresponds to $\omega_{\mathrm{EDM}}(t)$ whose data were taken for 10^4 s. The data points are fit to the sine function, and the sensitivity is calculated from the fit results. The sensitivity calculated with this method was about $10^{-31} e \cdot$ cm for frequencies $< 100~\mu$Hz. This method can be used for higher frequencies if one uses a shorter measurement time ($< 10^3$ s). No extra measurement is required for the axion search in this frequency region. One can do the static EDM experiment with frozen spin conditions and do the analysis for the axion signal search afterwards.

For higher frequencies, the resonance method can be used. Each run is done at a fixed frequency with the resonance conditions. In this case, the axion coherence time can be used as the measurement time for each storage time. Assuming the measurement time to be one axion coherent time for each frequency and 10^{11} particles per storage,

$SCT = 10^4$ s, and $Q_{ax} = 3 \times 10^6$, the sensitivities are calculated to be about $10^{-29} - 10^{-26} e \cdot$ cm.

In order to shorten the scan time, one can use a shorter measurement time. As an example, we tested each frequency for 3 s of measurement time, and Table III shows the sensitivity estimation results. 10^{11} particles were used for each measurement. We used the axion width, $\Delta f_{ax} = f_{ax}/Q_{ax}$, as the scan step. The total scan time can also be estimated by multiplying the measurement time of each frequency by the number of steps. The resulting total scan time was calculated to be about 2 yr for both 1 Hz–1 kHz and 1 kHz–1 MHz, respectively. For the higher-frequency range, 1–100 MHz, the total scan time is about 1.3 yr. The limit plot drawn based on the calculation results shown in Table III is presented in Fig. 7. The neutron EDM case is added for comparison (see Sec. VI for a detailed explanation). The average sensitivities were used for the limit plot for both the B-field ring and E/B combined ring.

The scan time estimation described above is based on resonance. However, one can utilize off-resonance signals to shorten the scan time. In Fig. 8, the simulation results show that the storage ring method is sensitive to the off-resonance case as well. The simulation was performed with the $g-2$ frequency of 100 kHz and assumed the axion frequency to be 2 Hz off the $g-2$ frequency. The measurement time was 30 s. One can clearly see the beat oscillation signal at 2 Hz which can be obtained from the FFT analysis as shown in Fig. 8(b). Figure 8(c) shows the FFT magnitude as a function of the axion frequency offset from the $g-2$ frequency. The off-resonance sensitivity decreases as the axion frequency moves away from the resonance [see the inset in Fig. 8(c)]. The sensitivity at resonance is estimated to be $4 \times 10^{-27} e \cdot$ cm at $f_{g-2} = 10^5$ Hz.

From this simulation study, we found that one can obtain sensitivities of $< 10^{-24} e \cdot$ cm within 0.002% offset of the $g-2$ frequency. Using $2 \times 0.002\%$ ($= 4 \times 10^{-5} f_{g-2}$) as the scan steps, the scan times are estimated to be 60 days for both 1 Hz–1 kHz and 1 kHz–1 MHz and 40 days for the scan range of 1–100 MHz. In this rough scan time estimation, we used the same measurement time of 30 s for the three frequency ranges. However, for precise calculations, the axion coherence time and spin coherence time should be considered for each frequency step. Then, the scan times for the high-frequency range will be shorter because of the short axion coherence time. In any case, the resulting scan time can be significantly reduced compared to the resonance scan case.

The off-resonance signal could be too small to be detected. However, recently, O'Hare et al. reported important results saying that a strong dark matter wind could be blowing in our region of the Galaxy [39]. If that is the case, there could be high chances of detecting strong axion signals.
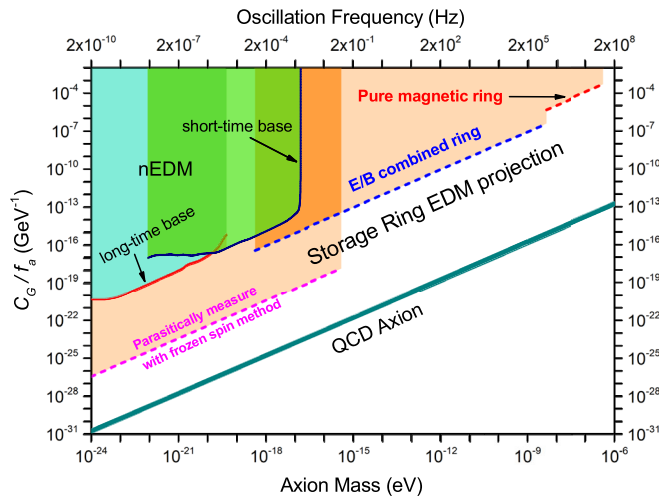

FIG. 7. Experimental limits for the frequency scan with deuterons. The measurement time is assumed to be 3 s for each frequency with an $E + B$ ring and axion coherence time with a B-field ring. See Table III for details.

VI. AXION GLUON COUPLED EDM SEARCHES AND THE SENSITIVITY OF THE EXPERIMENTS

The current experimental limit comes from the ultracold neutron trap method (NEDM) [40–44]. One can compare the sensitivities between the NEDM method and the storage ring EDM method. For example, the statistical error of the NEDM for one day's measurement is reported to be $6 \times 10^{-25} e \cdot$ cm (see [42] for details). This result is based on the experimental parameters such as the number of particles per storage (13 000 neutrons), a free precession time of 130 s, and an electric field of 450 kV/m. Compared with the proposed storage ring EDM method, the number of particles can reach up to 10^{11} per storage, the polarimeter efficiency can be about 2% for the proton or deuteron case, the effective electric field can be over 1 GV/m, and the

measurement time, which is limited by the spin coherence time, can be more than 10^4 s. For example, for the 10^5 Hz deuteron case with a measurement time of one day, the sensitivity is estimated to be $\sim 10^{-28} e \cdot$ cm. From this comparison, one can tell the storage ring method is more sensitive than the ultracold neutron trap method, by roughly more than 3 orders of magnitude.

However, NEDM collaborations have been pursuing efforts to improve sensitivity using a highly sensitive spectrometer that can improve sensitivity by 10 times the current record of $10^{-26} e \cdot$ cm. They expect to achieve an even higher sensitivity of $3 \times 10^{-28} e \cdot$ cm with an upgraded ultracold neutron source [45–49].

Figure 9 shows the experimental limits for the axion-gluon coupled oscillating EDM measurements. For
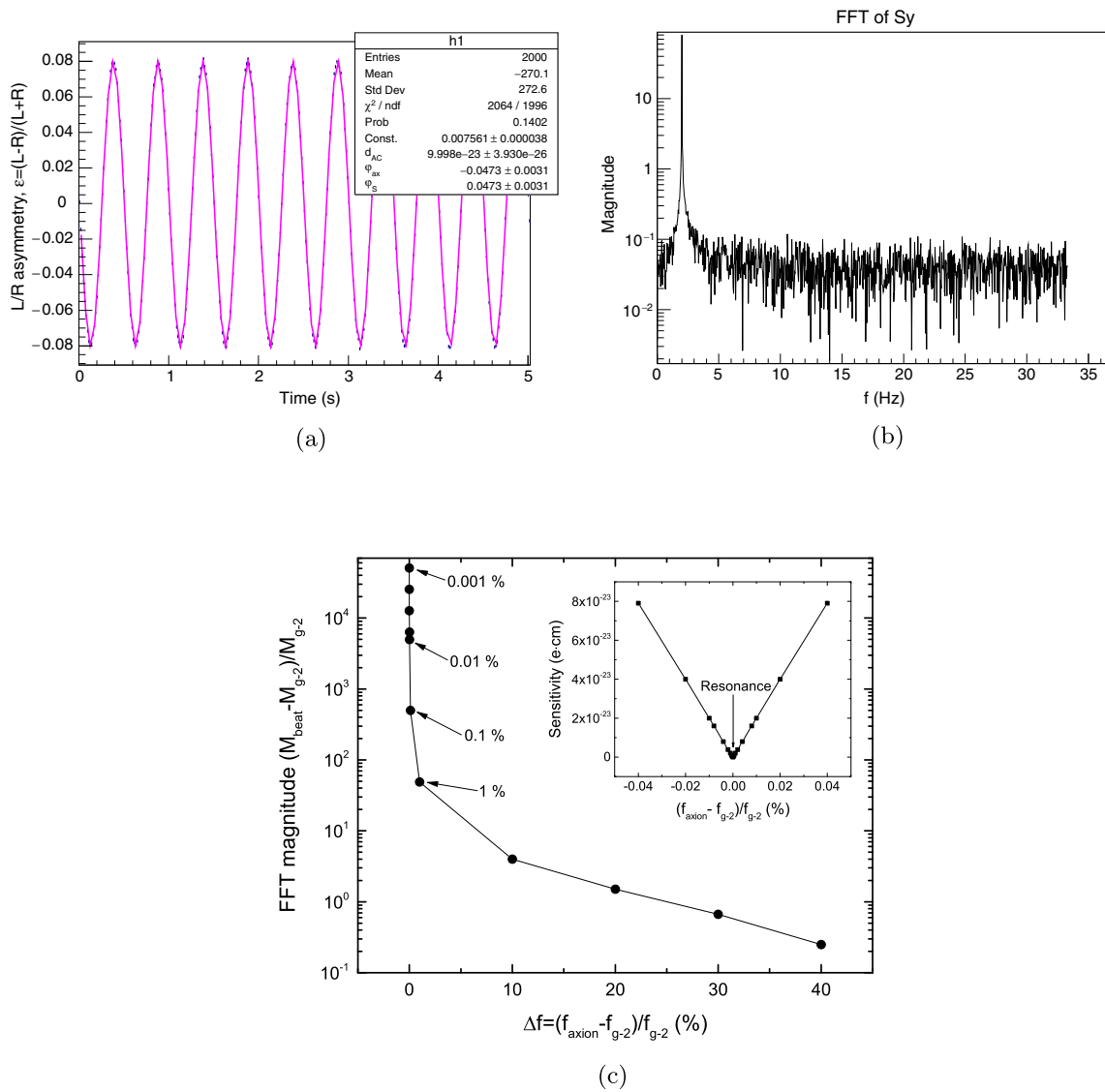

(a)

(b)

(c)

FIG. 8. Simulation results of the off-resonance mode. (a) Off-resonance oscillation signal. The tested $g - 2$ frequency is 10^5 *Hz* and the axion frequency is 2 *Hz* away from the $g - 2$ frequency. (b) FFT spectrum of Fig. 8(a). (c) FFT magnitude of off-resonance oscillation signal vs axion frequency offset from the $g - 2$ frequency.

comparison, we include the NEDM results, which were taken from Fig. 4 in Ref. [40]. Two sets of data are displayed for comparison. Two different time bases were used for the least squares spectral analysis (LSSA). The "long-time base" plot is an analysis of data collected from 1998 to 2002 (4 yr), and the "short-time base" is from the data taken with higher sensitivity from 2015 to 2016 (506 days). Here the terms long-time and short-time base imply different LSSA analysis steps used. For the long-time base analysis, the LSSA analysis step of 7.49 nHz (1/4 yr) was used, and 23 nHz (1/506 days) was used for the short-time base analysis. The details are described in the reference.

Based on the calculation results shown in Tables I and II, the projected limit of the storage ring EDM method is drawn by the red dotted line for the resonance method with the pure magnetic ring (1 MHz $< f_{ax} <$ 100 MHz), the blue dotted line with the E/B combined ring method (100 μHz $< f_a <$ 1 MHz), and the magenta dotted line for the frozen spin method ($f_{ax} <$ 100 mHz). For an axion frequency below 100 mHz, one can take data from the frozen spin condition which is used for the static EDM experiment. By combining many separate runs of data, as
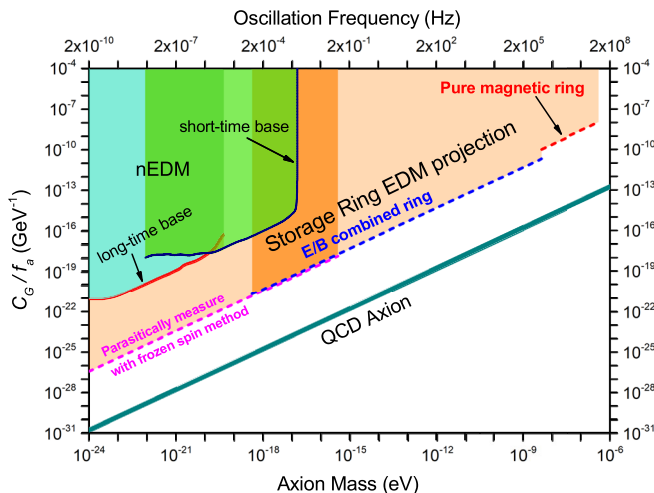

FIG. 9. Experimental limits for the axion-gluon coupled oscillating EDM measurement. The NEDM results are included for comparison. See Ref. [40] for detailed NEDM results. The limits for three different frequency regions are indicated with different colors of broken lines. Average values are used for each frequency region. See the column for SCT $= 10^4$ s and $Q_{ax1} = 3 \times 10^6$ in Tables I and II for the relevant numbers. If 10^{10} is used as the axion quality factor, the C_G/f_a can be improved by 1 or 2 orders of magnitude in the high-frequency region. An estimation of the limit plot for storage ring EDM method is made by assuming that the axion mass (frequency) is known, and the measurement is performed for 8×10^7 s at that frequency. However, for very low frequency ranges ($f_{ax} <$ 100 mHz), the axions can be searched for with high sensitivity using the frozen spin method without knowing the axion frequency. See the text for details.

the ultracold neutron EDM experiment did (periodogram analysis) [40], searching for the very low frequency region is possible. Even lower frequency searches are possible with data collected for longer times. The sensitivities used for the projected limit plot were averages for the SCT $= 10^4$ s and $Q_{ax1} = 3 \times 10^6$ in Tables I and II for the 100 MHz proton case.

The CASPEr experiment proposes cosmic axion searches using the nuclear magnetic resonance (NMR) method [50,51]. They utilized the resonance of nuclei spin precession with the oscillating axion field. With the NMR method, one can search the high-frequency region when a strong magnetic field is used.

The axion field is proportional to the square root of the local axion dark matter density. For this calculation, we used $\rho_{DM}^{local} \approx 0.3$ GeV/cm^3 as the local cold dark matter density. Furthermore, it can take advantage of the recently proposed local dark matter enhancement factors from the focusing effects due to planetary motion [52,53].

VII. SUMMARY AND CONCLUSION

As a candidate for dark matter, the axion has been the target of extensive searches using microwave cavities and other methods. The fact that the axion-gluon coupling can produce an oscillating EDM in nucleons led to the novel idea of measuring the oscillating EDM in hadronic particles like the proton and deuteron. We propose using the storage ring technique to measure the axion-induced oscillating EDM at the resonance conditions between the axion frequency and $g - 2$ spin precession frequency.

In this study, we calculated the electric field and magnetic field that are required for the resonance conditions. With the experimental conditions, we estimated the achievable sensitivities, and the result shows the experiment is more sensitive than the planned static EDM measurement ($10^{-29}e \cdot$ cm) by at least one order of magnitude, $\leq 10^{-30}e \cdot$ cm. This sensitivity is achieved if we assume that we know the axion frequency and spend all the experimental time at one frequency value. At very low frequencies, $f_{ax} <$ 100 mHz, one can search for the axion with the sensitivities of $\sim 10^{-31}e \cdot$ cm using the frozen spin method, without knowing the axion frequencies.

A wide range of frequencies (10^{-9} Hz $-$ 100 MHz) of axion dark matter can be searched by using both deuterons and protons in the same storage ring. Even though the proposed method does not reach the estimated sensitivity needed to reach the theoretical models of axion dark matter induced oscillating EDM, it promises to be one of the most sensitive ways to look for axions over a wide frequency range.

With the frozen spin conditions, systematic errors from an imperfect field alignment or residual B field are not canceled, and one needs to correct them using specific technologies [20,54]. However, with nonzero $g - 2$ precession, the four bunches of polarizations rotate and the

errors are canceled. This distinguishes an axion case, because the precession angle growth due to the axion signals with the four polarization bunches will accumulate in one direction. Since this method uses the interaction between the $g-2$ frequency and axion field induced oscillating EDM, once the $g-2$ frequency is well controlled, it is not necessary to know the precise momentum. The $g-2$ frequency is controllable at a precision level of 10^{-10} as mentioned in Sec. III.

APPENDIX: SENSITIVITY ESTIMATION RESULTS

As shown in Sec. III, the statistical error of the EDM d can be calculated from the fit of the experimental data with the Eq. (A1):

TABLE I. Examples of experimental parameters for frequency tuning and results of sensitivity calculation (deuteron). The analyzing power was assumed to be $A = 0.36$ if the momentum P was below 2 GeV/c, and $A = 0.15$ was used for the momentum $P > 2$ GeV/c. The ring bending radius was 10 m. The polarimeter efficiency was assumed to be 2%, and the initial polarization was 0.8. The axion quality factors are $Q_{ax1} = 3 \times 10^6$ and $Q_{ax2} = 10^{10}$.

					Sensitivity ($e \cdot$ cm)					
					SCT $= 10^3$ s		SCT $= 10^4$ s		SCT $= 10^5$ s	
B (T)	P (GeV/c)	f_{g-2} (Hz)	E_r (V/m)	E^* (V/m)	Q_{ax1}	Q_{ax2}	Q_{ax1}	Q_{ax2}	Q_{ax1}	Q_{ax2}
0.3800	0.9428	1.E1	8.82E6	4.23E7	9.9E-31	9.9E-31	3.1E-31	3.1E-31	9.9E-32	9.9E-32
0.3800	0.9429	1.E2	8.82E6	4.23E7	9.9E-31	9.9E-31	3.1E-31	3.1E-31	1.4E-31	9.9E-32
0.3800	0.9433	1.E3	8.80E6	4.24E7	9.9E-31	9.9E-31	4.3E-31	3.1E-31	3.8E-31	9.9E-32
0.3800	0.9473	1.E4	8.65E6	4.27E7	1.4E-30	9.9E-31	8.3E-31	3.1E-31	1.2E-30	9.9E-32
0.3800	0.9880	1.E5	7.05E6	4.60E7	3.5E-30	9.1E-31	3.5E-30	2.9E-31	3.5E-30	9.1E-32
0.3800	1.0345	2.E5	5.06E6	5.00E7	4.6E-30	8.4E-31	4.5E-30	2.7E-31	4.5E-30	9.8E-32
0.3800	1.1326	4.E5	3.47E5	5.85E7	5.5E-30	7.2E-31	5.5E-30	2.3E-31	5.5E-30	5.2E-32
0.3800	1.2386	6.E5	−5.47E6	6.82E7	5.8E-30	6.2E-31	5.3E-30	2.0E-31	5.8E-30	1.1E-31
0.3800	1.3546	8.E5	−1.26E7	7.93E7	5.7E-30	5.3E-31	3.9E-30	1.7E-31	5.7E-30	1.0E-31
0.3800	1.4836	1.E6	−2.14E7	9.20E7	5.5E-30	4.6E-31	3.5E-30	1.4E-31	5.5E-30	1.0E-31
0.8000	2.5124	1.E6	−9.13E6	2.01E8	1.6E-30	1.5E-31	2.5E-30	6.6E-32	2.5E-30	4.6E-32
0.9198	2.7574	1.E6	0.0	2.28E8	5.3E-30	4.4E-31	3.4E-30	1.4E-31	5.3E-30	9.7E-32
9.1977	27.5740	1.E7	0.0	2.75E9	3.3E-30	3.7E-32	4.4E-30	2.5E-32	4.4E-30	2.4E-32

TABLE II. Examples of experimental parameters for frequency tuning and results of the sensitivity calculation (proton). The analyzing power was assumed to be $A = 0.6$ for the momentum $P < 1$ GeV/c, and $A = 0.25$ was used for the momentum $P > 1$ GeV/c. The ring bending radius was 52 m for the E/B combined ring, and $r = 10$ m for the pure magnetic ring. The polarimeter efficiency used was 2%, and the initial polarization was 0.8. The axion quality factors are $Q_{ax1} = 3 \times 10^6$ and $Q_{ax2} = 10^{10}$.

					Sensitivity ($e \cdot$ cm)					
					SCT $= 10^3$ s		SCT $= 10^4$ s		SCT $= 10^5$ s	
B (T)	P (GeV/c)	f_{g-2} (Hz)	E_r (V/m)	E^* (V/m)	Q_{ax1}	Q_{ax2}	Q_{ax1}	Q_{ax2}	Q_{ax1}	Q_{ax2}
0.00011	0.6984	1.E1	−8.0E6	8.02E6	1.6E-30	1.6E-30	5.0E-31	5.0E-31	1.6E-31	1.6E-31
0.00010	0.6984	1.E2	−8.0E6	8.02E6	1.6E-30	1.6E-30	3.6E-31	3.6E-31	2.2E-31	1.6E-31
0.00008	0.6982	1.E3	−8.0E6	8.01E6	1.6E-30	1.6E-30	6.9E-31	5.0E-31	6.1E-31	1.6E-31
−0.00015	0.6960	1.E4	−8.0E6	7.97E6	2.2E-30	1.6E-30	1.9E-30	4.1E-31	1.9E-30	1.6E-31
−0.00243	0.6747	1.E5	−8.0E6	7.57E6	6.4E-30	1.7E-30	4.9E-30	5.3E-31	6.4E-30	1.7E-31
−0.00495	0.6519	2.E5	−8.0E6	7.15E6	9.6E-30	1.8E-30	9.5E-30	5.6E-31	6.7E-30	2.0E-31
−0.01523	0.7103	4.E5	−1.1E7	8.24E6	1.2E-29	1.1E-30	1.2E-29	4.8E-31	1.2E-29	2.3E-31
−0.02002	0.6711	6.E5	−1.1E7	7.51E6	1.6E-29	1.7E-30	1.4E-29	5.3E-31	1.6E-29	2.9E-31
−0.02666	0.6643	8.E5	−1.2E7	7.38E6	1.8E-29	1.7E-30	1.8E-29	5.4E-31	1.8E-29	3.4E-31
−0.03327	0.6583	1.E6	−1.3E7	7.27E6	2.1E-29	1.7E-30	2.1E-29	5.5E-31	2.1E-29	3.8E-31
0.36587	1.0968	1.E7	0.0	8.33E7	4.4E-29	3.6E-31	4.4E-29	1.9E-31	4.4E-29	2.4E-31
3.65868	10.9684	1.E8	0.0	1.09E9	2.3E-29	3.9E-32	3.4E-29	5.8E-32	3.4E-29	5.8E-32

TABLE III. Deuteron sensitivities for the 3 s measurement. The last raw is for proton. AP is the analyzing power, E^* the effective electric field, ω_{EDM} the spin precession rate, T_{cohe} the axion coherence time, and T_{meas} the measurement time.

f_{g-2} (Hz)	Ring type	AP	E^* (V/m)	ω_{EDM}	T_{cohe} (s)	T_{meas} (s)	Sensitivity ($e \cdot$ cm)
1.0E1	$E+B$	0.36	4.23462E + 07	−3.2E-07	300000	3	6.2E-26
1.0E2	$E+B$	0.36	4.23499E + 07	−3.2E-07	30000	3	6.2E-26
1.0E3	$E+B$	0.36	4.23822E + 07	−3.2E-07	3000	3	6.2E-26
1.0E4	$E+B$	0.36	4.27061E + 07	−3.2E-07	300	3	6.1E-26
1.0E5	$E+B$	0.36	4.60434E + 07	−3.5E-07	30	3	5.7E-26
2.0E5	$E+B$	0.36	4.99613E + 07	−3.8E-07	15	3	5.2E-26
4.0E5	$E+B$	0.36	5.85416E + 07	−4.4E-07	7.5	3	4.5E-26
6.0E5	$E+B$	0.36	6.82496E + 07	−5.2E-07	5	3	3.8E-26
8.0E5	$E+B$	0.36	7.93095E + 07	−6.0E-07	3.75	3	3.3E-26
1.0E6	$E+B$	0.36	9.20350E + 07	−7.0E-07	3	3	2.8E-26
1.0E6	B	0.15	2.27994E + 08	−1.7E-06	3	3	2.8E-26
1.0E7	B	0.15	2.75104E + 09	−2.1E-05	0.3	0.3	7.2E-26
1.0E8	B	0.25(P)	1.09285E + 09	−1.7E-05	0.03	0.03	1.7E-24

$$\sigma_d = \frac{s\hbar}{E^*}\sigma_{\omega_d}, \tag{A1}$$

where s is $1/2$ for protons and 1 for deuterons, E^* the effective electric field, and ω_d is the vertical spin precession rate. We estimated the sensitivity of the experiment using this formula with appropriate experimental parameters. Three spin coherence times and two axion quality factors are considered in the calculations as examples. Table I and II show the sensitivity estimation results for deuteron case and proton case, respectively. Table III is the sensitivity estimation results for deuterons calculated with 3 s of measurement time. The details are described in the text.

[1] R. D. Peccei and H. R. Quinn, Phys. Rev. Lett. **38**, 1440 (1977).
[2] S. Weinberg, Phys. Rev. Lett. **40**, 223 (1978).
[3] F. Wilczek, Phys. Rev. Lett. **40**, 279 (1978).
[4] J. E. Kim, Phys. Rev. Lett. **43**, 103 (1979).
[5] M. Shifman, A. Vainshtein, and V. Zakharov, Nucl. Phys. **B166**, 493 (1980).
[6] A. R. Zhitnitsky, Sov. J. Nucl. Phys. **31**, 260 (1980).
[7] M. Dine, W. Fischler, and M. Srednicki, Phys. Lett. **104B**, 199 (1981).
[8] J. Kim, S. Nam, and Y. Semertzidis, Int. J. Mod. Phys. A **33**, 1830002 (2018).
[9] P. W. Graham, I. G. Irastorza, S. K. Lamoreaux, A. Lindner, and K. A. van Bibber, Annu. Rev. Nucl. Part. Sci. **65**, 485 (2015).
[10] P. Sikivie, Phys. Rev. Lett. **51**, 1415 (1983).
[11] P. W. Graham and S. Rajendran, Phys. Rev. D **84**, 055013 (2011).
[12] P. W. Graham and S. Rajendran, Phys. Rev. D **88**, 035023 (2013).
[13] J. Choi, H. Themann, M. J. Lee, B. R. Ko, and Y. K. Semertzidis, Phys. Rev. D **96**, 061102 (2017).
[14] J. Jeong, S. Youn, S. Ahn, J. E. Kim, and Y. K. Semertzidis, Phys. Lett. B **777**, 412 (2018).
[15] J. Jeong, S. Youn, S. Ahn, C. Kang, and Y. K. Semertzidis, Astropart. Phys. **97**, 33 (2018).

[16] N. Du et al. (ADMX Collaboration), Phys. Rev. Lett. **120**, 151301 (2018).
[17] Y. K. Semertzidis, Precision physics in the storage ring: Probing old and new physics, Axion dark matter, available at https://www.perimeterinstitute.ca/videos/precision-physics-storage-rings.
[18] V. Anastassopoulos et al., A proposal to measure the proton electric dipole moment with 10^{-29} e · cm. Sensitivity by the Storage Ring EDM Collaboration (2011), available at https://www.bnl.gov/edm/files/pdf/Proton_EDM_proposal_20111027_final.pdf.
[19] D. Anastassopoulos et al., AGS proposal: Search for a permanent electric dipole moment of the deuteron nucleus at the 10^{-29} e · cm level (2008), available at https://www.bnl.gov/edm/files/pdf/deuteron_proposal_080423_final.pdf.
[20] V. Anastassopoulos et al., Rev. Sci. Instrum. **87**, 115116 (2016).
[21] G. Guidoboni et al. (JEDI Collaboration), Phys. Rev. Lett. **117**, 054801 (2016).
[22] V. Bargmann, L. Michel, and V. L. Telegdi, Phys. Rev. Lett. **2**, 435 (1959).
[23] J. D. Jackson, Classical Electrodynamics, 3rd ed. (Wiley, New York, 1999).
[24] G. G. Ohlsen, Rep. Prog. Phys. **35**, 717 (1972).
[25] G. G. Ohlsen and P. Keaton, Nucl. Instrum. Methods **109**, 41 (1973).

[26] B. Bonin *et al.*, Nucl. Instrum. Methods Phys. Res., Sect. A **288**, 389 (1990).

[27] H. O. Meyer, G. L. Moake, and P. P. Singh, Phys. Rev. C **23**, 616 (1981).

[28] N. Brantjes *et al.*, Nucl. Instrum. Methods Phys. Res., Sect. A **664**, 49 (2012).

[29] P. Marmier and E. Sheldon, in *Physics of Nuclei and Particles* (Academic, New York, 1970), pp. 1019–1086.

[30] L. Krauss, J. Moody, F. Wilczek, and D. E. Morris, Phys. Rev. Lett. **55**, 1797 (1985).

[31] M. S. Turner, Phys. Rev. D **42**, 3572 (1990).

[32] P. Sikivie, arXiv:1009.0762.

[33] P. Sikivie, Phys. Lett. B **567**, 1 (2003).

[34] D. Eversmann *et al.* (JEDI Collaboration), Phys. Rev. Lett. **115**, 094801 (2015).

[35] Y. Satou *et al.*, Phys. Lett. B **549**, 307 (2002).

[36] V. Ladygin *et al.*, Nucl. Instrum. Methods Phys. Res., Sect. A **404**, 129 (1998).

[37] M. McNaughton *et al.*, Nucl. Instrum. Methods Phys. Res., Sect. A **241**, 435 (1985).

[38] W. J. Marciano, Brookhaven National Laboratory, USA (private communication).

[39] C. A. J. O'Hare, C. McCabe, N. W. Evans, G. Myeong, and V. Belokurov, Phys. Rev. D **98**, 103006 (2018).

[40] C. Abel *et al.*, Phys. Rev. X **7**, 041034 (2017).

[41] K. Green, P. G. Harris, P. Iaydjiev, D. J. R. May, J. M. Pendlebury, K. F. Smith, M. van der Grinten, P. Geltenbort, and S. Ivanov, Nucl. Instrum. Methods Phys. Res., Sect. A **404**, 381 (1998).

[42] P. G. Harris *et al.*, Phys. Rev. Lett. **82**, 904 (1999).

[43] C. A. Baker *et al.*, Phys. Rev. Lett. **97**, 131801 (2006).

[44] C. Baker *et al.*, Nucl. Instrum. Methods Phys. Res., Sect. A **736**, 184 (2014).

[45] P. Schmidt-Wellenburg, AIP Conf. Proc. **1753**, 060002 (2016).

[46] Y. Kermaidic, in *Proceedings of the 12th Conference on the Intersections of Particle and Nuclear Physics (CIPANP 2015), Vail, Colorado, USA, 2015* (2015).

[47] T. M. Ito *et al.*, Phys. Rev. C **97**, 012501 (2018).

[48] T. E. Chupp, P. Fierlinger, M. J. Ramsey-Musolf, and J. T. Singh, Rev. Mod. Phys. **91**, 015001 (2019).

[49] K. K. H. Leung *et al.*, arXiv:1903.02700.

[50] D. Budker, P. W. Graham, M. Ledbetter, S. Rajendran, and A. O. Sushkov, Phys. Rev. X **4**, 021030 (2014).

[51] A. Garcon *et al.*, arXiv:1707.05312.

[52] K. Zioutas *et al.*, arXiv:1703.01436.

[53] S. Bertolucci, K. Zioutas, S. Hofmann, and M. Maroudas, Phys. Dark Universe **17**, 13 (2017).

[54] S. Haciomeroglu and Y. K. Semertzidis, Phys. Rev. Accel. Beams **22**, 034001 (2019).